Sanfeliu Cano, C.; Martínez-Máñez, R.; Sancenón Galarza, F.; Soto Camino, J.; Amoros Del Toro, PJ.; Marcos Martínez, MD. (2015). Ceramic foam supported active materials for boron remediation in water. Desalination. 374:10-19. doi:10.1016/j.desal.2015.06.020.

Ceramic foam supported active materials for boron remediation in water.

Cristina Sanfeliu,[abc] Ramón Martínez-Máñez,[abc] Félix Sancenón,[abc] Juan Soto,[abc] Pedro Amorós,[d] Mª Dolores Marcos.[abc *]

[a] Centro de Reconocimiento Molecular y Desarrollo Tecnológico (IDM), Unidad Mixta Universitat Politècnica de València, Universitat de València, Spain.
[b] Departamento de Química, Universitat Politècnica de València, Camino de Vera s/n E-46022 Valencia, Spain. (Tel.: (+34) 963877343)
[c] CIBER de Bioingeniería Biomateriales y Nanomedicina (CIBER-BBN), Spain.
[d] Institut de Ciència del Materials (ICMUV), Universitat de València, P.O. Box 22085, E-46071, Valencia, Spain. (Tel.: (+34) 963543617)
*Corresponding Author: mmarcos@qim.upv.es.

Abstract

Due to the narrow range between boron necessities and toxicity in the environment, there is a high interest in the design of effective boron remediation procedures. We have previously reported a promising boron adsorption material based on the affinity of boron aqueous species for cis-diol groups that were anchored on different mesoporous silica matrices. However, the small particle size of these systems makes them difficult to be applied on real remediation situations. In this context we report herein a novel system for boron adsorption from aqueous solutions in which the high boron affinity for functionalized mesoporous materials is combined with the mechanical properties of ceramic foams as macroscopic supports. The efficiency of these new composites for boron removal is very high and comparable with the parent microparticulated adsorbent.

Introduction

Boron is widely distributed in the environment, mainly in the form of borate salts which are very soluble and hence difficult to remove from water. The principal boron contamination is due to industrial wastewater discharge as for example the ceramic industry. In regions with a high concentration of such industries the contamination of ground and subsoil by boron is considered of maximum environmental concern [1].

Boron is an important micronutrient for plants, animals and humans. It has a marked effect on plants in terms of both nutrition and toxicity, even 1-2 ppm in irrigation water can cause stunting of plant growth. Boron also has virulence for reproduction and causes disease in the nervous system of animals and humans [2, 3]. Therefore, removal of boron from water is crucial for boron environmental protection.

The World Health Organization (WHO) guidelines for water quality recommend a 2.4 mgL^{-1} standard for boron in drinking water [4]. In the case of the European Union (EU) a standard of $1mgL^{-1}$ for drinking water [5] for boron has been adopted, though in some countries derogations have been made due to a higher boron concentration in natural fresh water [6].

There is no universal method for the removal of boron from water [7]. Main processes for boron removal include adsorption [8, 9], coagulation [10], reverse osmosis [11-14], electrodialysis [15], etc. The adsorption process is extensively used [16, 17]. Therefore, novel materials and methods are being developed [18].

Previously, we presented an alternative system: a new generation of boron adsorption materials based on functionalized mesoporous silica [19]. This method was developed taking advantage, in one side, of

the boron ability to produce esters with chemical compounds containing multiple hydroxyl groups (polyols) [20, 21] and, on the other, of the attractive properties of mesoporous solids such as very large capacity of functionalisation and very high specific surface [22, 23]. Based on these ideas, it was envisaged that the grafting of mesoporous scaffolds with saccharides could yield highly efficient boron removal systems. Several of these mesoporous scaffolds with different porous structures have been obtained and compared with non-porous inorganic materials and though the best adsorption result was obtained for highly homogeneous scaffolds, other cheap matrices showed also a good performance [24].

However, thinking on real applications, the relatively small particle size of these functionalized mesoporous materials constitute a significant disadvantage. At this point, we will pointed out that the grain size of the inorganic silicas we have used (50-300 nm) is significantly lower than the size of other materials used for boron remediation such as Dianion or Dowex ion exchange resins (in the micrometric-milimetric range) [25-27].The solid-liquid separation process becomes hard and difficult when nanometric particles are involved. This drawback can be solved by the incorporation of the active species onto a macroscopically structured support. In this context, ceramic foams (CF) represent an emerging category of hosts that possess a unique combination of physicochemical (high porosity and chemical stability) and mechanical (low thermal-expansion coefficients and high specific strength) properties [28-30]. In addition, CF can be easily manufactured by impregnation of organic template foams with inorganic particles or by in situ polymerization followed by calcination [31].

Preparation and characterization of "CF-mesoporous silica" composites in the form of rigid large monoliths having trimodal pore systems (small meso-, large meso-, and macroporous) has been described [32]. The monoliths have been synthesized by using preformed mesoporous nanoparticles and a CF as support. The surfactant-assisted synthesis of the silica-based nanoparticulate mesoporous materials, denoted as **UVM-7** (a nanometric version of the MCM-41 silicas), has been reported elsewhere [33]. These **UVM-7** materials show very open architectures consisting of micrometric aggregates of mesoporous nanoparticles connected through covalent bonds.

In this study, we present a novel system for boron adsorption from aqueous solutions in which the high accessibility of the UVM-7 mesoporous materials has been combined with the boron affinity towards diols and the mechanical properties of the ceramic foams as macroscopic supports. The efficiency of this new system in boron removal is also presented.

Experimental

Synthesis of the adsorbents

The synthesis of the ceramic foam (CF) was carried out through a typical organic foam replication, a technique that allows good control of the monolith shape and dimensions [34]. Commercially available inexpensive polyurethane foam (PUF) without cell forming membranes (average pore diameters around 600 μm (30 ppi)) was used as macro-scale template. The foam was impregnated with an optimally deflocculated casting slip for porcelain bodies prepared with two different kaolins, feldspar and quartz, which contained 67% of solid materials (19.4% kaolin A, 18.1% kaolin B, 10.7% quartz, 18.8% feldspar), and 33% of water, which included the deflocculant (0.45% with respect to solid kaolins), to give a slip density of 1.6 g/cm^3. As deflocculant, a mixture of sodium carbonate ($Na_2CO_3 \cdot 10H_2O$) and sodium silicate (aqueous solution with a density of 1.36) in a weight ratio of 2:1 was used. The green body obtained with this slip had the following chemical composition: SiO_2, 68.0%; Al_2O_3, 21.5%; Na_2O, 0.8%; K_2O, 4.1%; ignition loss, 5.6%; distributed as kaolinite, quartz, and feldspar minerals. The impregnated PUF was passed through rollers preset at 80% compression to expel the excessive slurry and dried at room temperature to obtain a coated PUF. Then, the monolith was calcined in a two-step process (at 500 °C for 2 h, and later at 1200° for 5 h) to provoke PUF evolution and ceramic vitrification. The corresponding porcelain body contains two crystalline phases, mullite and quartz, and a vitreous phase containing sodium and potassium aluminosilicates.

The nanosized mesoporous UVM-7 silica was synthesized through a one-pot surfactant-assisted procedure using a homogeneous hydroalcoholyc reaction medium (water/triethanolamine).The general

procedure, a modification of the so-called atrane route [35], has been described in detail elsewhere. It is based on the use of a simple structural directing agent ((CTABr) cetyltrimethylammonium bromide) and a complexing polyalcohol (triethanolamine), which originates silatrane complexes (relatively inert complexes that include triethanolamine-related ligand species) as hydrolytic precursors. Together with its complexing ability, the presence of the cosolvent (triethanolamine) was a key in order to favor the formation of nanoparticulated materials. To open the intrananoparticle mesopores, the surfactant was extracted from the as-synthesized mesostructured solid by chemical exchange using an HCl/ethanol solution (CTA^+/H^+ exchange). Thus, 1 g of mesostructured UVM-7 powder was suspended in a solution containing 16 mL of HCl (37%) and 130 mL of ethanol (99%), and this mixture was heated at reflux (60 °C) for 2 h while stirring. Later, after renewal of the HCl/ethanol solution, and to complete the extraction process, the suspension was heated again at 60 °C for 16 h while stirring. The resulting mesoporous solid **UVM-7-e** was collected by filtration, washed with ethanol, and air-dried at 100 °C.

The large aggregates of **UVM-7-e** material were transformed into submicrometric or nanometric aggregates by means of high power ultrasound treatment (using a Branson instrument). In a typical preparation, a suspension containing 3g of **UVM-7-e** in 100 mL of distilled water (3% in weight) was irradiated for 15 min at a nominal power of 350 W. After irradiation, the suspension has colloidal character showing the Tyndall effect. The CF coating was performed by successive impregnation cycles. In each cycle an immersion of the ceramic foam into an aqueous **UVM-7-e** colloidal suspension (ca. 3% in weight) was firstly performed, and afterwards, a soft thermal treatment (150 °C for 16 h) to favor water evolution and nanoparticles adhesion (formation of covalent Si-O-Si bonds with the CF surface). The solid **CF-UVM-7-e** was hence obtained. Mesoporous material anchored to the monolith was functionalised in order to build the active sites on the materials surface [36]. **CF-UVM-7-e** monoliths were immersed in anhydrous acetonitrile (500 ml) and heated at 120 ºC in a Dean-Stark apparatus to remove the adsorbed water by azeotropic distillation under an inert atmosphere (Ar gas). After this, 25.6 mmol (6ml) of APTES ((3-aminopropyl)-triethoxysilan), were added and the solution was stirred for 16h. Then, the monoliths (**CF-UVM-7-N**) were washed with acetonitrile, and ethanol. Finally, 0.5 L of a 0.07M solution of gluconolactone in methanol was added to the former mixture, and after stirring for 48 hours at room temperature the fully functionalized monoliths, named **CF-G** (**-a**, **-b**, **-c** for those used for adsorption essays and **–d**, **-f** , **–g**, to be used in the different analytical techniques), were achieved.

In order to compare the adsorption capacity of the supported active materials, a non-supported **UVM-7-e** material was also functionalized. Hence, 2 g of **UVM-7-e** were suspended in 70 ml of acetonitrile and heated at 120ºC in a dean-stark apparatus. Then, 3.4 mmol of APTES were added at room temperature following the same conditions as those described above for the **CF-UVM-7-e**. After 16 h., the solid was filtered and washed with acetonitrile and water reaching to **UVM-7-N**. Finally, in order to achieve the active sites **UVM-7-N** material was reacted with 6.8 mmol of gluconolactone in 100 ml of methanol. The mixture was stirred during 48h at room temperature. After that, the obtained **S1** solid was filtered, washed with water and dried. A summary of the codes used for naming the prepared materials and composites.

Table 1. Summary of the codes used for the prepared materials and composites.

CF	Non functionalised ceramic foam
UVM-7	Non functionalised mesostructured silica (including the template surfactant)
UVM-7-e	Non functionalised mesoporous silica (surfactant extracted)
CF-UVM-7-e	Ceramic foam coated with non functionalised mesoporous silica
CF-UVM-7-N	3-aminopropyl-functionalised mesoporous silica coated ceramic foam
CF-G-a	Fully functionalised mesoporous silica coated ceramic foam (including glucose moiety) –used in adsorption assays
CF-G-b	Fully functionalised mesoporous silica coated ceramic foam (including glucose moiety) –used in adsorption assays
CF-G-c	Fully functionalised mesoporous silica coated ceramic foam (including glucose moiety) –used in adsorption assays
CF-G-d	Fully functionalised mesoporous silica coated ceramic foam (including glucose moiety) –for analysis
CF-G-f	Fully functionalised mesoporous silica coated ceramic foam (including glucose moiety) –for analysis
CF-G-g	Fully functionalised mesoporous silica coated ceramic foam (including glucose moiety) –for analysis
UVM-7-N	3-aminopropyl-functionalised mesoporous silica
S1	Fully functionalised mesoporous silica (including glucose moiety)

Boron adsorption assays

Adsorption studies of boron on **CF-G** were carried out dipping each monolith in 25 ml of distilled water while stirring. After two hours, an aliquot of 2 ml was extracted from the solution and another 2 ml aliquot of 75 ppm of boron was added resulting in a nominal concentration of 6 ppm of boron. Thus, every two hours an aliquot of 2 ml was extracted from the solution in contact with the monolith and another 2 ml aliquot of increasing boron solution was added in order to keep a constant volume of 25 ml. This protocol was kept on until the concentration of the solution reached 230 ppm with the aim of reaching the monolith saturation for boron adsorption. Boron adsorption studies on **S1** were carried out suspending 30 mg of **S1** solid in 12.5 ml of boron solution at a certain concentration in order to maintain the same conditions as those in the **CF-G** functionalisations. The suspensions were stirred during 16 h. and then the mixture was filtered. The boron concentration in the solutions was analyzed by azomethine-H as a colorimetric reagent according to the method described in references [37, 87].

Kinetic adsorption studies of boron on **CF-G** were carried out dipping the monolith in 25 ml of a 5 ppm boron solution. An aliquot of 1 ml was extracted from the solution at different times during 4h. Batch experiments were carried out for kinetic assays on the **S1** solid. These involved suspension of 30 mg of **S1** solid in 12.5 ml of a 5 ppm boron solution in order to maintain the same conditions as for **CF-G** material. The suspensions were stirred and an aliquot was taken and filtered at different times during 4h. Boron concentration was determined using Perkin Elmer Spectrophotometer with azomethine-H method [37,38].

Characterization Techniques

X-ray powder diffraction (XRD) data were recorded on a Bruker D8 Advance diffractometer using Cu Kα radiation. Both low- and high-angle XRD patterns were recorded to analyze the diffraction signals typical of the UVM-7 mesoporous silicas and the peaks associated with the ceramic foam. Low angle XRD patterns were collected in steps of 0.02°2θ over the angular range 0.65-10°2θ and an acquisition time of 25 s/step. High-angle patterns were collected with a scanning step of 0.05°2θ over the angular range of 10-70°2θ and an acquisition time of 10 s/step. High and low-magnification SEM images were recorded by using a Jeol JSM 6300 microscope. Samples were previously coated with Au-Pd. A TEM study was carried out with a Philips CM10 instrument operating at 100 kV and equipped with a CCD camera. Samples were gently ground in dodecane, and microparticles were deposited on a holey carbon film supported on a Cu grid. Nitrogen adsorption-desorption isotherms (-196 °C) were recorded with a Micromeritics ASAP- 2010 automated instrument. Calcined samples were degassed at 120 °C and 10^{-6} Torr for 5h prior to measurement. Surface areas were estimated according to the BET model, and pore size dimensions and pore volumes were calculated by using the BJH method from the adsorption branch of the isotherms. Particle size measurements (DLS) were performed using a Malvern Zetasizer ZS instrument. Thermogravimetric analyses were carried out on a TGA/SDTA 851e Mettler Toledo balance, with a heating program consisting of a heating ramp of 10°C per minute from 393 to 1273 K and an isothermal heating step at this temperature over 30 min. Spectrophotometric measurements were carried out with a Lambda 35 UV/Vis Spectrometer from Perkin–Elmer Instruments.

Results and discussion

Preparation of the adsorbent agents

As we have commented in the introduction, the system for boron adsorption we have designed is based on the capacity of boron ions to form boro-esters with molecules that present consecutive diols. Hence, our idea was to obtain an adsorbent material with the highest possible concentration of diols. This point can be easily reached by functionalisation of mesoporous silicas with saccharides moieties due to the high surface area these materials present and its ease functionalization. However, two important points must be also taken into account in order to get a good performance of the final adsorbent. In first

place, the active sites (consecutive diols) should present maximum accessibility. This feature can be attained when using the materials denoted as UVM-7 as the mesoporous support. These materials are a nanometric version of the MCM-41 silicas and show very open architectures consisting of micrometric aggregates of mesoporous nanoparticles connected through covalent bonds. This organization defines two pore systems: the first one (intraparticle) is generated by the effect of the surfactant micelles and the second one (inter-particles) is formed as the nucleation and growth of the primary mesoporous nanoparticles proceeds. In this way, an improved accessibility to the active sites can be attained without losing the possibility of a high surface functionalisation of the mesoporous materials. The surfactant-assisted synthesis of the UVM-7 silica-based nanoparticulated mesoporous materials has been reported elsewhere [33].

The second point to be contemplated to get a good performance of the adsorption system was the improvement of the adsorbent handling as the mesoporous materials usually are obtained as very fine powders (in the nanometric range) and then are not good candidates for real adsorption processes. In this case, the opted solution was to choose ceramic foam as macroscopic inorganic support. Hence, the final adsorption system would be composed by a mesoporous silica matrix that after being supported on macroporous ceramic foam is being functionalized with saccharide moieties.

Additionally, the large aggregates of the as-synthesized **UVM-7-e** silica can be transformed into even smaller sub-micrometric or nanometric aggregates by means of high-power ultrasound treatment, which leads to stable colloids in water [39]. This is a key point in our preparative procedure because it allows us to have stable **UVM-7-e** colloidal particles able to cover the **CF** support by dip coating. Besides, **UVM-7-e** materials so treated still maintain the same high capacity to be easily derivatized with functional groups. [40] Then, the poliol group selected as the binding site will be attached to the silica framework by prior reaction with an alkoxysilane reactant.

The preparation of **CF-G** composites is shown in Scheme 1. The coating process of the **CF** support was performed by successive impregnation dip-coating cycles into an aqueous **UVM-7-e** colloidal suspension (ca. 3% in weight) followed by soft thermal treatment (150 °C for 16 h) to favor water evolution and nanoparticle adherence (formation of covalent Si-O-Si bonds both among nanoparticles and with the **CF** surface). The resulting monoliths **CF-UVM-7-e** were then weighted and the amount of impregnated material was determined to be approximately 0.05 g of UVM-7 per monolith (a mean value of 6.4% of increment). Then, surface organic functionalization was carried out through a two steps grafting protocol. The starting **CF-UVM-7-e** was first reacted with (3-aminopropyl)-triethoxysilane in acetonitrile to yield **CF- UVM7-N**, and then with gluconolactone in methanol to obtain the final **CF-G** composite. After the full functionalisation process an average increment of mass of 7.9% corresponding meanly to the adhered **UVM-7-G** active material was obtained. In Table 2 the main values for the coating and functionalisation process performed on several **CF** matrices are collected. It can be seen that even when the process presents some difficulties due to the mixing of three different phases, **CF** support, **UVM-7** mesoporous solid and the components in the aqueous solution, the results on Table 1 show a quite acceptable reproducibility of the synthetic process.

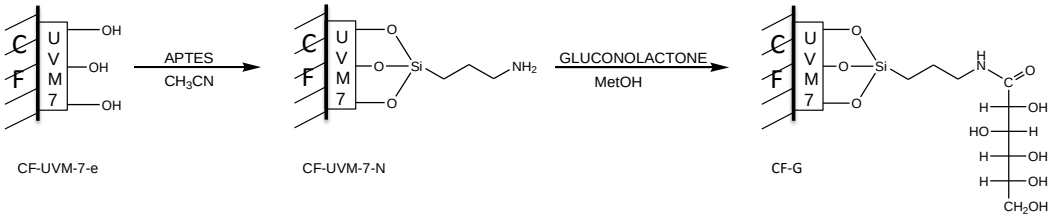

Scheme 1. Route for the preparation of **CF-G** composites.

Table 2. CF coating and functionalization process for several **CF-G** monoliths.

	Initial mass (g)	1st adhesion of UVM-7-e (g)	2nd adhesion of UVM-7-e (g)	UVM-7-e adhered (%wt)	Final mass (g)[a]	UVM7-G adhered (% wt)[b]
CF-G-a	0.8816	0.9060	0.9293	5.13	0.9435	6.56
CF-G-b	0.8777	0.8999	0.9234	4.95	0.9362	6.25
CF-G-c	0.6716	0.6968	0.7168	6.31	0.7378	8.97
CF-G-d	0.4550	0.4732	0.4912	7.37	0.4940	7.89
CF-G-f	0.6662	0.6972	0.7242	8.01	0.7407	10.06
CF-G-g	0.6101	0.6250	0.6550	6.85	-	-

[a] Mass of the monolith after complete functionalisation

[b] Percentage of active material **UVM7-G** adhered in the final monolith.

The non-supported **UVM-7-e** material was also functionalized following the same procedure: the silica mesoporous powder was treated with APTES in acetonitrile to yield **UVM-7-N** and then the resulting solid was treated with gluconolactone in methanol to yield **S1**. In this way, the adsorbent capacity of **CF-G** materials, in which the active mesoporous particles are stuck on the ceramic foam, can be compared with the capacity of the non-supported **S1** material directly suspended in water.

Materials characterization

The inorganic material used as macroscopic support for the active material is a macroporous solid that can be described as ceramic foam (**CF**). This scaffolding was prepared through conventional polyurethane foam (PUF) replica technique described by Schwartzwalder [31], which allows good control of the macroscopic monolith shape and dimensions. As expected from the SiO_2-Al_2O_3 phase diagram, the XRD data (Fig. 1) show that the final material is basically formed by two crystalline phases, quartz (60%) and mullite (23%) (estimated composition from XRD phase analysis), and a vitreous phase including amorphous sodium and potassium aluminosilicates. The result is a rigid foamlike macroporous monolith (**CF**) (wt % composition, after calcination: SiO_2 72.0%, Al_2O_3 22.8%, Na_2O 0.9%, K_2O 4.3%). While it might be assumed that this monolith with high percentage of silica could be a good candidate for functionalizing directly with APTES and later with gluconolactone, there are two reasons to discard this strategy: its very low surface area (0.001 m^2/g) and the difficulty to anchor APTES groups considering the high degree of condensation of the monolith (as expected taking into account the high temperatures employed in its synthesis). Both factors, separately, and even more cooperatively, would lead to a material with low content of functional groups and consequently with a low capacity to capture boron species. Therefore, to increase the surface and facilitate the functionalization, we includes within the monolith a siliceous material of high surface area, easy to functionalize (due to its amorphous nature) and having small grain size (to invade easily the macropores of the monolith). These features are provided by the UVM-7 silica.

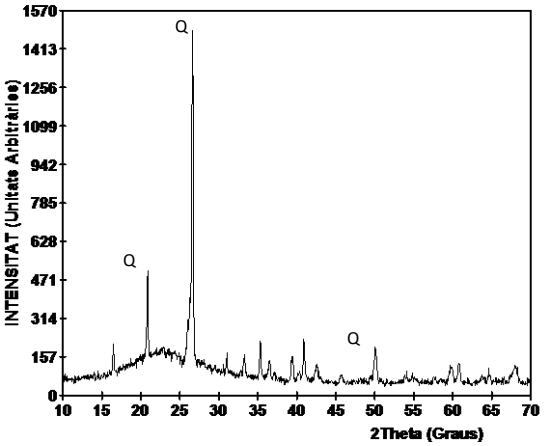

Figure 1. XRD pattern of the ceramic foam (**CF**). Q = quartz. The remaining peaks correspond to mullite.

The mesoporous and hybrid materials were characterized by standard procedures. X-ray diffraction (XRD) patterns of the materials **UVM7**, **UVM-7-e** and **CF-UVM-7-e** (Fig. 2) show that the intense peak at about 2°2θ, characteristic of surfactant-assisted mesoporous materials, does not suffer major changes, that is, the synthetic steps do not significantly affect the mesoporous structure of the silica mesoporous matrix even after the sticking process on the ceramic foam.

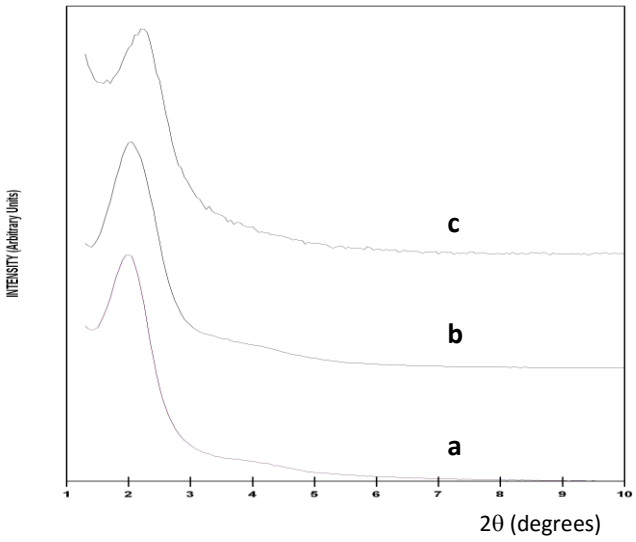

Figure 2. Low angle powder XRD patterns of (a) **UVM7**, (b) **UVM-7-e** and (c) **CF-UVM-7-e**.

The transformation of the large aggregates of the as-synthesized **UVM-7-e** solid into smaller sub-micrometric or nanometric aggregates after high power ultrasound treatment can be easily followed by direct observation. Indeed, after ultrasound irradiation, the suspension acquired colloidal character showing the Tyndall effect. Additionally, the decrease of the aggregate dimensions was studied by transmission electron microscopy. In Figure 3 representative TEM images of **UVM-7-e** material before and after ultrasound irradiation are shown. However, a more direct evidence of the true particle size that interacts with the ceramic support (and its evolution) is obtained by DLS. Thus, we measured the grain size of the UVM-7 silica dispersions (with concentration identical to that used in the impregnation cycles) before and after sonication. A decrease of the aggregate sizes from 830 to 220 nm is induced through ultrasound irradiation (Figure 4). The low grain size achieved is adequate to ensure an efficient invasion along the macropores of the monolith.

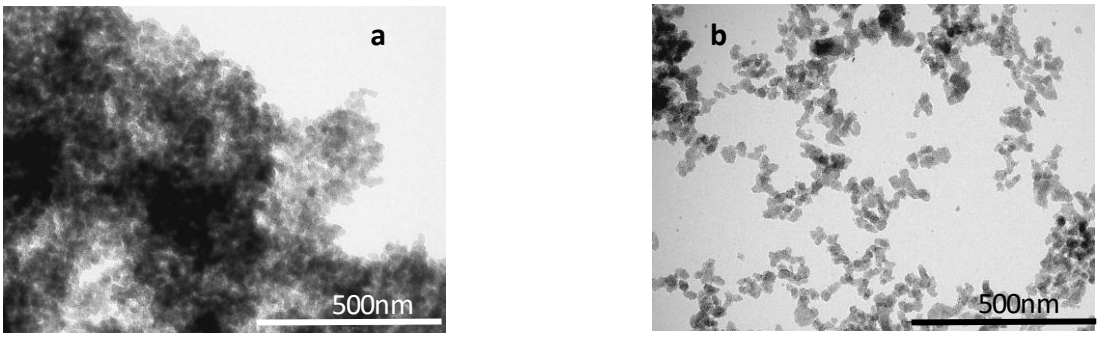

Figure 3. TEM micrographs of the **UVM-7-e** aggregates before (a) and after (b) ultrasound irradiation.

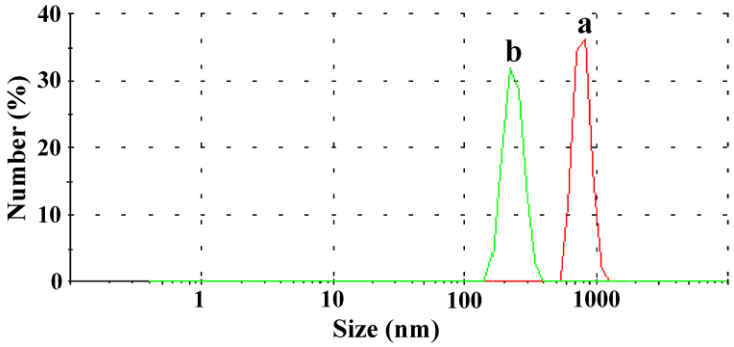

Figure 4. DLS curves of the **UVM-7-e** aggregates before (a) and after (b) ultrasound irradiation.

The coating process leading to **CF-UVM-7-e** can be appreciated in Figures 5 to 8. In Figure 5 an optical image of the ceramic foam before and after the coating process is shown. A closer insight of the coating process is shown in Figure 6 where Scanning Electron Microscope (SEM) images reveal the differences produced on the monolith surface during the process. The foam coating is rather homogeneous and can be described as formed by successive deposition of small **UVM-7-e** flakes in an imbricate way. These flakes are rather regular and have about 6-9 μm of thickness. The origin of these thick flakes is likely due to cracks generated during the drying process. Probably, the macrostructure generated by superposition of the **UVM-7-e** flakes induces a "binder" effect favoring the cohesion of the particles among them. High-magnification SEM and TEM images (Figure 7) demonstrate that the **UVM-7** organization is preserved. Thus, at micrometric scale, the deposited silica flakes present rough surfaces (Figure 7a) consisting of aggregates of pseudospherical clusters of mesoporous nanoparticles (Figure 7b), which define true textural large mesopores among them. The intraparticle disordered small mesopore system can be clearly appreciated in Figure 7b. This fact confirms that the intraparticle mesopore organization is preserved after the **CF** coating. These mesopore systems (small and large) typical of **UVM-7** mesoporous material, together with the foam-like interconnected macropores (400-600 μm) define a very open hierarchical porous architecture.

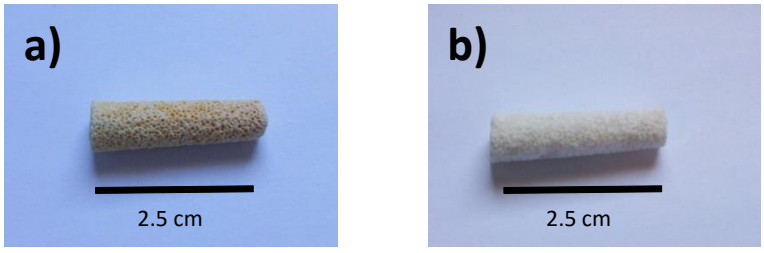

Figure 5. Optical images: (a) Starting foam, (b) **CF-UVM-7-e** composite.

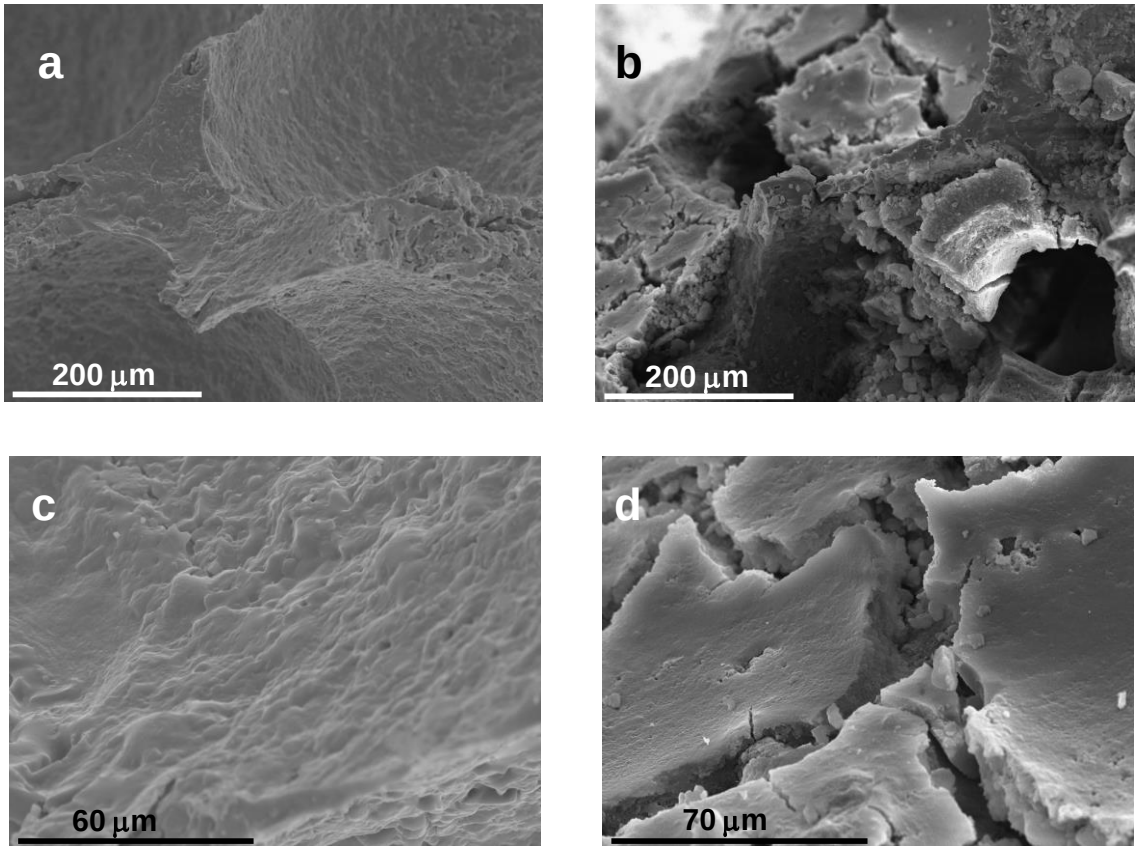

Figure 6. SEM images of the **CF**: (a) and (c) before coating, and (b) and (d) after two impregnation cycles.

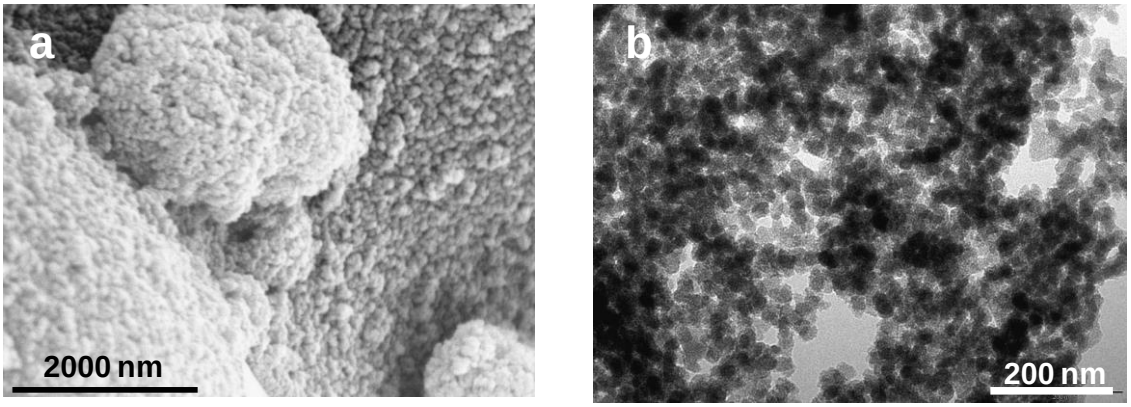

Figure 7. SEM (a) and TEM (b) images showing typical **UVM-7** like aggregates of the mesoporous nanoparticles present in the **CF** monolith after two impregnations.

SEM image in Figure 8 shows the interior (transverse section) of a CF-coated monolith. Thus, it can be appreciated that the coating efficiency gets into the deepest part of the monolith and that the deposition of **UVM-7-e** particles is not limited to the exterior of the ceramic foam. In practice there are no appreciable differences in the coating degree between the monolith surface and its interior.

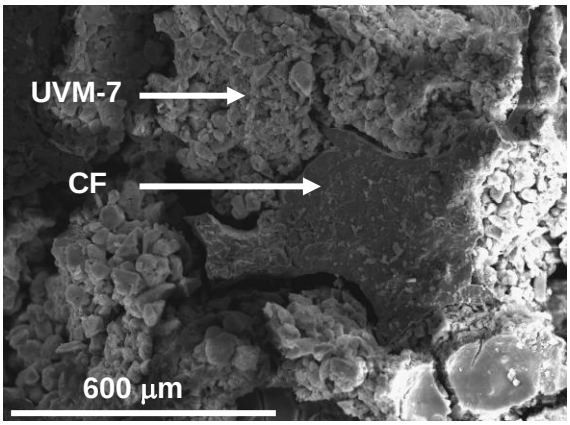

Figure 8. SEM image of a section of the **CF** after two impregnation cycles with **UVM-7-e.**

In Figure 9, the evolution of the N_2 adsorption with the ceramic foam impregnation process is shown. Isotherms of the resulting composites show the characteristic features of UVM7 materials: two well-defined adsorption steps at intermediate ($0.3 < P/P0 < 0.5$) and high ($P/P0 > 0.8$) relative pressure values, which can be respectively associated with the filling of the intra-nanoparticle (surfactant generated) small mesopores and the interparticle (generated by condensation of the primary nanoparticles) large mesopores.

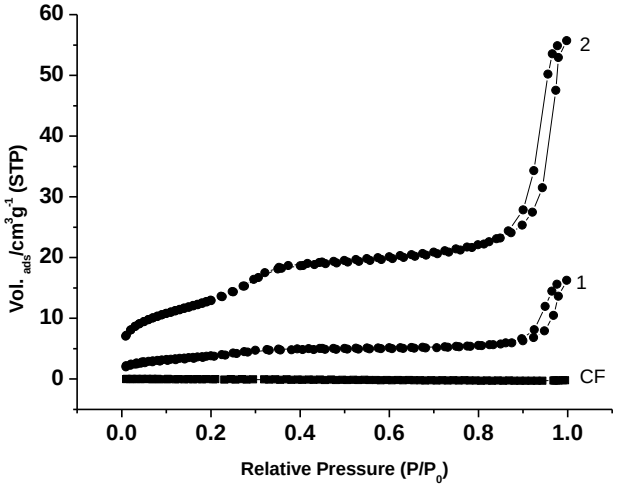

Figure 9. N_2 isothermal absorption/desorption curves for: CF) non-impregnated ceramic foam; 1) ceramic foam after one UVM-7-e impregnation cycle; and 2) ceramic foam after two UVM-7-e impregnation cycles.

The physisorption data in Table 3 evidence that both the BET surface area, calculated from a Brunauer–Emmet–Teller (BET) treatment of the isotherms [41], and volumes and the pore sizes, estimated by the Barrett–Joiner–Halenda (BJH) method [42], in the composite monoliths increase with the number of impregnation cycles. Moreover, the N_2 adsorption ratio associated with the intra- and interparticle pores reminds that expected for a **UVM-7** mesoporous material. After two cycles, the weight increase for the **CF** analyzed (**CF-G-g**, Table 1) was 6.85%, which corresponds to the incorporation of 0.045 g of **UVM-7-e** material. Assuming that the 47.1 m^2/g are basically due to the adhered **UVM-7-e** solid, we can estimate an average BET area of 687.1 m^2/g for the mesoporous active phase prior the final

functionalisation. This value fits very well with typical BET area of **UVM-7** bulk phases. Then, the high accessibility of the **UVM-7** pore system is preserved even for nanoparticles close to the **CF** surface.

Table 3. Evolution of the textural properties and coverage level for UVM-7 mesoporous coated CF composites

	Coating cycles	BET (m^2/g)	BJH intraparticle pore (nm)	BJH interparticle pore (nm)	Small pore volume (cm^3/g)	Large pore volume (cm^3/g)	Relative impregnation[a]	UVM7 content[b] (% wt)
UVM-7-e	-	877.7	2.73	48.6	0.71	1.58	-	-
CF	0	0.001	-	-	-	-	0	0
CF-UVM-7-e	1	13.7	2.43	43.3	0.01	0.02	2.44	2.38
CF-UVM-7-e	2	47.1	2.69	33.5	0.04	0.06	7.35	6.85

[a] increment of mass of the monolith after each impregnation process (referred to the initial monolith weight)
[b] Percentage of UVM-7 adhered in the CF- UVM-7-e monolith.

The functionalisation degree of **CF-G** monoliths and **S1** material was also assessed by elemental analysis and thermogravimetric studies. From the elemental contents (C, H, N), the amount of *N-(3*-triethoxysilylpropyl)gluconamide groups were calculated. In order to compare both type of solids the final functionalisation value is given as millimoles per mass unit of silica residue (α_{amine} in mmol of amine/g SiO_2, and $\alpha_{glucose}$ in mmol of glucose/g SiO_2). Hence, for **S1** solid the silica residue was taken directly from thermogravimetric analysis. In the case of **CF-G** the data was taken from the thermogravimetric decomposition of the **CF-G-f** monolith and taking into account the amount of **UVM-7-G** adhered onto the corresponding **CF** support. The final functionalization value was referred to the silica residue of the adhered **UVM-7-e**. In this way, even when both materials **CF-G-f** and **S1** are quite different, their functionalisation degree can be compared. Functionalisation data are collected in Table 4. It can be seen that **CF-G-f** and **S1** present different functionalisation degree, while **S1** solid contain 1.29 mmol of amino groups per gram of SiO_2, **CF-G-f** composite has 2.79 mmol of amino groups per gram of SiO_2 (silica residue of the active **UVM-7-e** adhered material). The contents on saccharide groups for both materials follow a similar tendency, **S1** solid has lower functionalisation (0.77 mmol of saccharide groups per gram of SiO_2) while **CF-G-f** has higher amount of glucose groups (1.31 mmol of saccharide groups per gram of SiO_2). These differences in the functionalisation degree could be related with the different availability of reactants during the preparation of both materials. Even when the concentration of reactants (APTES and gluconolactone) are initially the same in both processes, the differences in shape and size between the initial supports, **CF-UVM-7-e** and microparticulated **UVM-7-e**, compelled us to use a higher amount of the corresponding solutions for the functionalisation of the monoliths, and so higher amount of reactants were available in this case.

However the higher funtionalisation of the **CF** composite, from the values of these α factors the difference in the yield of the reaction between the amino groups and glucolactone says that the final reaction has lower effectiveness in the case of the ceramic foam **CF-G-f** (48%) than in the case of the microparticulated **S1** solid (60%). This fact could indicate that the access to the amine groups is somehow more intricate in the case of the ceramic foam.

Table 4. Amine and glucose contents and estimated average coverage for selected adsorbents

Adsorbent	Total amine (mol)	Total glucose (mol)	Amine (mmol/g UVM7-G)	glucose (mmol/g UVM7-G)	α_{amine} (mmol/g SiO_2)	$\alpha_{glucose}$ (mmol /g SiO_2)	$\alpha_{glucose}/\alpha_{amine}$ (%)[d]	$\beta_{glucose}$ (molecules /nm^2)
CF-G-f	0.0163	0.0079	1.625[a]	0.786[a]	2.70[b]	1.31[b]	48	0.88[c]
S1	0.1003	0.0600	1.003	0.560	1.29	0.77	60	0.52

[a] Amine or glucose content of the adsorbent per mass unit of the active material UVM7-G.
[b] Amine or glucose content of the adsorbent per mass unit of SiO_2 of the active material UVM7-G.
[c] Glucose coverage of the adsorbent taking into account the surface of the active material UVM7-G.
[d] Yield of the second functionalization reaction.

Boron sorption assays

Boron removal in functionalised materials is due to the complex formation between the boric acid and polyol groups incorporated into the pore structure of the sorbents. Although the reaction between gluconamide groups and boric acid molecules is not yet well clarified, boron is expected to form both bidentate and bisbidentate complexes with the consecutive alcohol groups of the glucose moieties attached to the surface of the adsorbent, as it is shown in Figure 10. Hence, functionalised materials will show the ability to remove boron from aqueous solutions depending meanly on the amount and distribution of the glucose groups on the adsorbent surface. In order to evaluate the adsorption capacity of the supported active material, both types of absorbents, monoliths and mesoporous solid **S1,** have been tested for their boron sorption efficiency.

First parameter to be studied has been the variation of boron adsorption for both **CF-G** and **S1**as a function of the contact time and the results are depicted in Figure 11. The experiment shows a very quick adsorption of boron by **S1** solid as the 90% of the total adsorption was reached already during the first minute at the experimental conditions used. Then, the adsorption levels off after approximately 15 minutes. In comparison, it takes longer time, around 15 minutes, to **CF-G-d** to get the same 90% level of adsorption and it is not after 40 minutes that the monolith-supported material reaches the maximum level of adsorption. This different behavior may be related with the unlike pathways in both adsorbents for boric moieties to reach the active sites. In the case of **S1** adsorbent the active material is directly suspended in the solution while in the case of **CF-G-d** composite boric moieties have to travel through the intricate structure of the monolith to reach the active groups.

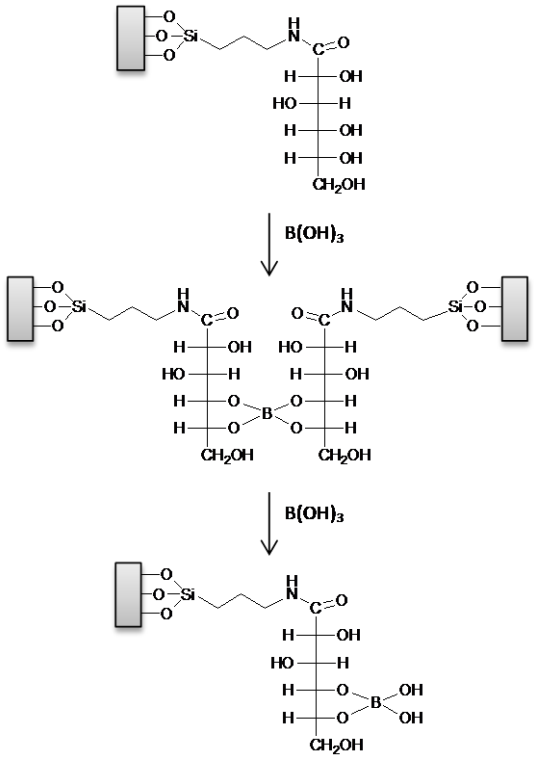

Figure 10. Proposed mechanism for the boron sorption by gluconamide-functionalized sorbents.

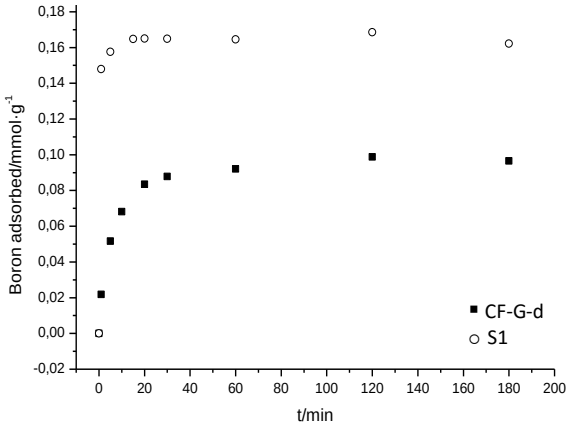

Figure 11. Evolution of the boron removal from a 5ppm B solution as a function of the contact time.

The borate adsorption behaviour for three monoliths (**CF-G-a**, **CF-G-b** and **CF-G-c**) and for **S1** are shown in Figure 12 (a and b respectively) where the amount of boron adsorbed per unit mass of the sorbent (in the case of monoliths, per unit mass of supported **UVM-7** already functionalized with the glucose) is shown as a function of the initial boron in solution. As can be seen from the curves, the amount of adsorbed boron increased as the boron equilibrium concentration in solution increased. The behaviour of the three monoliths is quite similar though different to the **S1** material as the monoliths take longer in reaching the saturation level.

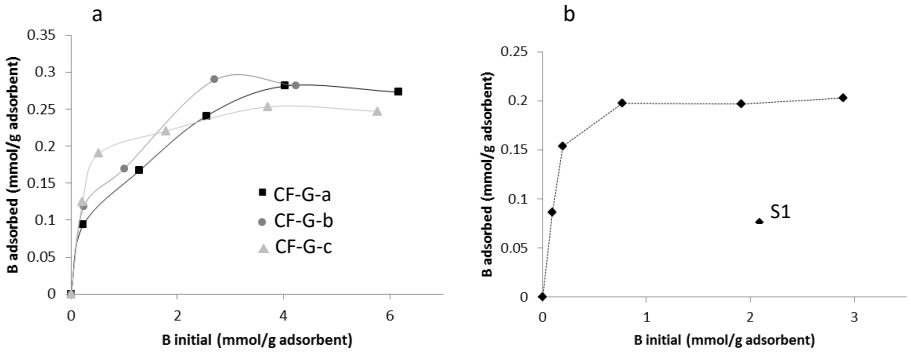

Figure 12. Boron adsorbed at 25ºC as function of the initial boron concentration a) for three different monoliths **CF-G-a**, **CF-G-b**, **CF-G-c** and b) for **S1**.

In a typical boron adsorption test, increasing amounts of boron were added to the solution in contact with the monolith while adsorbed boron was monitored. Saturation is reached at about 0.25 mmol of boron per gram of adsorbent. Consequently, bearing in mind the amount of saccharide present in the solid (see Table 3) it is possible to say that approximately a 32% of the binding sites are occupied. However, as each boron atom could be bonded to two glucose molecules the adsorption is not so far from full occupancy. Figure 12.b shows the performance of the material **S1** in boron adsorption. Batch studies were carried out for the adsorption assays. In this case, the saturation is reached with much lower equilibrium concentration and so, the isotherm reaches the saturation very fast. Yet, the occupancy of the available binding sites when saturation is reached behaves similarly as in the case of monoliths. In **S1** the 36% of the binding sites were occupied and thinking in a boron coordination through two glucose molecules, the system approaches the full occupancy.

In order to clarify the design of adsorption systems to remove boron species from aqueous solution, it is necessary to establish the most appropriate correlation for adsorption results. Several models have been

published in the literature to describe experimental data of adsorption isotherms. In this work, Langmuir model was used to describe the relationship between the adsorbed amount of boron and its concentration in solution at the equilibrium conditions. The Langmuir isotherm is valid for monolayer sorption onto a surface with a finite number of identical sites and uniform adsorption energies. This model assumes that the isotherm coverage can be expressed in terms of the Langmuir adsorption constant (K) and the concentration C_e (in mol/L) of the adsorbate at the equilibrium:

$$\Theta t = \frac{\mathrm{K} \cdot Ce}{1 + \mathrm{K} \cdot Ce}$$

On the other hand, experimental coverage can be expressed by the following equation:

$$\Theta e = \frac{Cs}{Cm}$$

where C_m is the maximum sorption capacity corresponding to the complete monolayer coverage (mmol/g) and C_s is the amount of adsorbed boron (mmol/g). In Figure 13 the plot of experimental coverage (θe) as a function of the equilibrium boron concentration in solution is presented and a typical Langmuir type adsorption can be appreciated.

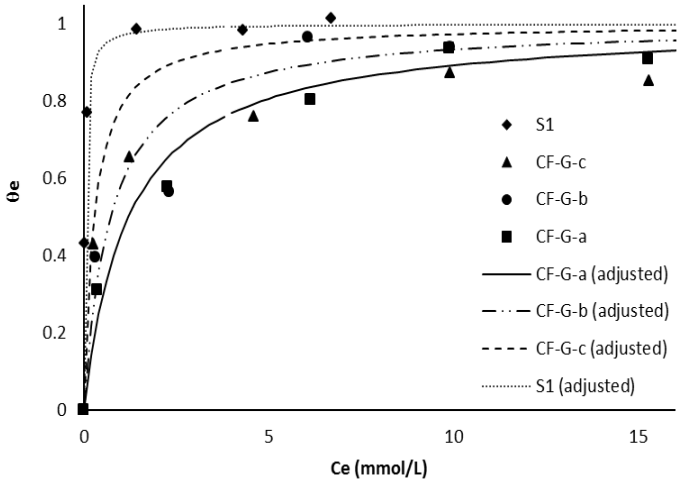

Figure 13. Boron adsorption isotherms for **S1** solid and **CF-G-(a, b,c)** monoliths.

From the adjustment of the Figure 13 plots using the Langmuir model values of the adsorption constant (K) and the monolayer capacity (C_m) for the different monoliths and **S1** can be obtained (see Table 5). The calculations have been performed with the Solver tool inside the Excel program by minimizing the quadratic average error between the theoretical (θ_t) and experimental coverage (θ_e). It can be seen that the three monoliths present similar constant values, with log K around 3. However, solid **S1** shows a constant with a value one order of magnitude higher. Bearing in mind that the adsorption constant accounts for the interaction between the adsorbent and the adsorbate, we could say that the synthesis of the active material (glucose functionalized **UVM-7** material) onto the ceramic foam induces a decrease in the interaction strength. The main difference between the two systems we have essayed in this paper is that the organic groups, that give rise to the final active sites, have different pathways until they reach the surface of the corresponding inorganic matrix where they must anchor. This fact, that has been already discussed above when talking about the yield of the functionalization reactions, may have influenced also the final distribution of the glucose groups attached onto the surface. If the gluconamide groups had a somehow more intricate pathway towards the anchored amines in the case of the ceramic foam the resulting glucose groups may present some steric hindrance for the borate groups to form bisbidentate complexes and a higher amount of only bidentate complexes would form during the boron

adsorption on **CF-G**. Hence, a different distribution of the glucose groups on the inorganic matrix could account for the differences in the constant values of the **CF-G** and **S1** materials.

Table 5: Langmuir constants

Adsorbent	Log K	C_m (mmol/g)	R^2
S1	4,48	0.20	0,9994
CF-G-a	2,91	0.30	0,9782
CF-G-b	3,10	0.29	0,9203
CF-G-c	3,25	0.25	0,9886

According with our previous studies, the active material **UVM-7-G** could be regenerated by simple acidic washing which quantitatively would remove the loaded boron because of the hydrolysis of the boron esters generated during the adsorption process. In order to corroborate the regeneration possibility of our new composites, a monolith (**CF-G-c**) was immersed into 100mL of 0.1 M HCl solution and left there for 24 hours at room temperature. Then the monolith was extracted from the acidic solution and washed with distilled water until the acid was completely removed. It was then treated with a fresh boron solution under the same conditions as in the first adsorption test and the adsorbed boron was measured as before. This process was repeated several times. Figure 14 shows a plot of the adsorption capacity of **CF-G-c** over successive cycles. It is observed that approximately 50% of initial boron sorption capacity can be preserved after the acidic treatment. The fact that the complete sorption capacity cannot be recovered could be related with the loss of poorly attached active sites during the acidic washing, as the more intricate morphology of the monoliths matrix may present more difficulties when producing a good functionalization of the surface. However, we remark that after the observed leaching of active sites (and the subsequent B adsorption decrease) during the first cycle, the material adsorption capacity is maintained in successive cycles.

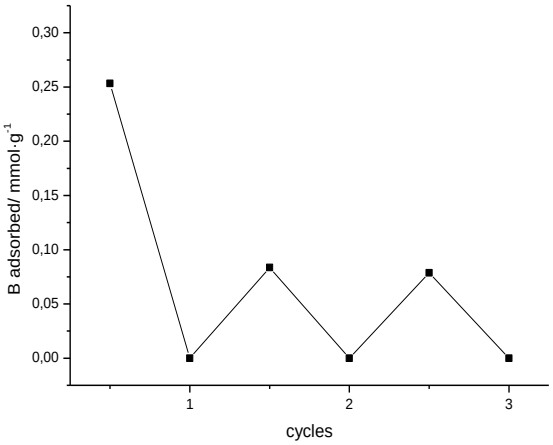

Figure 14. Evolution of the boron content for **CF-G-c** during several cycles of washing with HCl and boron adsorption.

Conclusions.

We have shown that ceramic monoliths can act as proper supporting matrices to get a boron adsorbent easier to handle for applied porpoises. The synthesis of this kind of composites shows a good reproducibility as all the monoliths essayed present similar behavior and adsorption properties. When comparing the **CF-G** composites with the parent adsorbent **S1**, monoliths present lower adsorption kinetics however they show comparable total adsorption capacity though at low boron concentrations the adsorption capacity is lower than for **S1**. The affinity of borate entities for the active sites in **CF-G** materials is lower than that for **S1** which may indicate a different distribution of the active sites onto the

CF-G composites related with a higher difficulty during the functionalization process due to a more intricate pathway for the organic moieties to reach the mesoporous surface. The capacity of **CF-G** composites to be recycled for new uses is quite good and makes of this material a promising candidate to be essayed in a continuous boron elimination process.

Acknowledgements

Financial support from the Spanish Government (Project MAT2009-14564-C04-01 and MAT2009-14564-C04-04, and MAT2012-38429-C04-01 and MAT2012-38429-C04-02) and the Generalitat Valenciana (Project PROMETEO/2009/016) is gratefully acknowledged. C.S. thanks the MICINN for a predoctoral fellowship.

References.

[1] P.W.Howe, A review of boron effects in the environment, Biol. Trace Elem. Res. 66 (1998) 153–166.
[2] R.F. Moseman, Chemical Disposition of Boron in Animals and Humans, Environ. Health Perspect. Suppl. 102 (1994) 113.
[3] V.M. Shorrocks, The occurrence and correction of boron deficiency, Plant Soil, 193 (1997) 121-148.
[4] WHO, Guidelines for drinking-water quality, 4th ed., Malta, 2011. (ISBN 978 92 4 154815 1)
[5] E.Weinthal, Y. Parag,A. Vengosh,A. Muti,W. Kloppmann, TheEUdrinkingwater directive: the boron standard and scientific uncertainty, Eur. Environ. 15 (2005) 1–12.
[6] SCHER (Scientific Committee on Health and Environmental Risks) scientific opinion on request for derogations on the Drinking Water Directive (Directive 98/83/EC), 16 April 2010.
[7] Y. Xu, Jia-Qian Jiang., Technologies for Boron Removal, Ind. Eng. Chem. Res. 47 (2008) 16-24.
[8] C. Yan,W. Yi, P. Ma, X. Deng, F. Li, Removal of boron from refined brine by using selective ion exchange resins, J. Hazard. Mater. 154 (2008) 564–571.
[9] C. Jacob, Seawater desalination: boron removal by ion exchange technology, Desalination 205 (2007) 47–52.
[10] A.E. Yilmaz, R. Boncukcuoglu, M.M.Kocakerim,M.T. Yilmaz, C. Paluluoglu, Boron removal from geothermal waters by electrocoagulation, J. Hazard. Mater. 153 (2008) 146–151.
[11] L. Melnyk, V. Goncharuk, I. Butnyk, E. Tsapiuk, Development of the sorption-membrane "green" technology for boron removal from natural and wastewaters, Desalination 205 (2007) 206–213.
[12] M. Turek, P. Dydo, J. Trojanowska, A. Campen, Adsorption/co-precipitationreverse osmosis system for boron removal, Desalination 205 (2007) 192–199.
[13] W. Bouguerra, A. Mnif, B. Hamrouni, M. Dhahbi, Boron removal by adsorption onto activated alumina and by reverse osmosis, Desalination 223 (2008) 31–37.
[14] N. Ozturk, D. Kavak, T.E. Kose, Boron removal fromaqueous solution by reverse osmosis, Desalination 223 (2008) 1–9.
[15] Y. Oren, C. Linder, N. Daltrophe, Y. Mirsky, J. Skorka, O. Kedem, Boron removal from desalinated seawater and brackish water by improved electrodialysis, Desalination 199 (2006) 52–54.
[16] T.E. Kose, N. Ozturk, Boron removal from aqueous solutions by ion-exchange resin: column sorption-elution studies, J. Hazard. Mater. 152 (2008) 744–749.
[17] S. Karahan, M. Yurdakoc, Y. Seki, K. Yurdakoc, Removal of boron from aqueous solution by clays and modified clays, J. Colloid Interface Sci. 293 (2006) 36–42.
[18] D.I. Fried, A. Schlossbauer, T. Bein, Immobilizing glycopyranose on mesoporous silica via ''click-chemistry'' for borate adsorption, Microporous and Mesoporous Materials 147 (2012) 5-9.
[19] G. Rodríguez-López, M.D. Marcos, R. Martínez- Máñez, F. Sancenón, J. Soto, L. A. Villaescusa, D. Beltrán and P. Amorós, Efficient boron removal by using mesoporous matrices grafted with sacchrides, Chem. Commun. (2004) 2198-2199.
[20] D. Yu, D. Xue, Bond analyses of borates from the inorganic crystal structure database, Acta Crystallogr. B62 (2006) 702–709.
[21] B. M. Smith, J. L. Owens, C. N. Bowman, P. Todd, Thermodynamics of borate ester formation by three readily grafted carbohydrates, Carbohydrate Research 308 (1998) 173-179
[22] J. Aguado, J. M. Arsuaga, A. Arencibia, M. Lindo, V. Gascón, Aqueous heavy metals removal by adsorption on amine-functionalized mesoporous silica, Journal of Hazardous Materials 163 (2009) 213–221.
[23] C. Coll, R. Martínez-Máñez, M. D. Marcos, F. Sancenón, J. Soto, and R. K. Mahajan, Efficient Removal of Anionic Surfactants Using Mesoporous Functionalised Hybrid Materials, Eur. J. Inorg. Chem. (2009) 3770–3777.
[24] C. Sanfeliu, R. Martínez-Máñez, F. Sancenón, J. Soto, V. Puchol, P. Amorós, M. D. Marcos, Low-cost materials for boron adsorption from water, J. Mat. Chem., 22, (2012), 25362-25372.
[25] N. Kabaya, S. Sarp, M. Yuksel, M. Kitis, H. Koseoglu, Ö. Arar, M. Bryjak, R. Semiat, Removal of boron from SWRO permeate by boron selective ion exchange resins containing N-methyl glucamine groups, Desalination 223 (2008) 49–56.
[26] N. Kabaya, I. Yilmaz-Ipek, I. Soroko, M. Makowski, O. Kirmizisakal, S. Yag, M. Bryjak, M. Yuksel. Removal of boron from Balcova geothermal water by ion exchange-microfiltration hybrid process, Desalination 241 (2009) 167-173.
[27] E. Güler, N. Kabay, M. Yüksel, N.Ö. Yigit, M. Kitis, M. Bryjak, Integrated solution for boron removal from seawater using RO process and sorption-membrane filtration hybrid method, Journal of Membrane Science 375 (2011) 249–257.
[28] P. Colombo, Novel processing of silicon oxycarbide ceramic foams, Adv. Eng. Mater. 1 (1999) 203–205.
[29] M.V. Twigg, J.T. Richardson, Theory and Applications of Ceramic Foam Catalysts, Chemical Engineering Research and Design 80 (2002) 183-189.
[30] A. Zamperi, P. Colombo, G.T.P. Mabande, T. Selvam, W. Schwieger, F. Scheffler, Zeolite Coatings on Microcellular Ceramis Foams: A Novel Route to Microreactor and Microseparator Devices, Adv. Mater., 16 (2004) 819-823.
[31] K. Schwartzwalder, H. Somers, A. V. Somers, U.S. Patent 3090094 (1963).

[32] L. Huerta, J. El Haskouri, D. Vie, M. Comes, J. Latorre, C. Guillem, M. D. Marcos, R. Martínez-Mañez, A. Beltrán, D. Beltrán, P. Amorós, Nanosized Mesoporous Silica Coatings on Ceramic Foams: New Hierarchical Rigid Monoliths, Chem. Mater. 19 (2007) 1082-1088.

[33] J. El Haskouri, D. Ortiz de Zárate, C. Guillem, J. Latorre, M. Caldés, A.Beltrán, D. Beltrán, A. B. Descalzo, G. Rodríguez, R. Martínez-Máñez, M. D. Marcos, P. Amorós, Silica-based powders and monoliths with bimodal pore systems, Chem. Commun. (2002) 330-331.

[34] K. Schwartzwalder, A. V. Somers, Method of Making a Porous Shape of Sintered Refractory Ceramic Articles, U.S. Patent 3090094 (1963).

[35] S. Cabrera, J. El Haskouri, C. Guillem, J. Latorre, A. Betrán, D. Beltrán, M.D. Marcos, P. Amorós, Generalised syntheses of ordered mesoporous oxides: the atrane route, Solid State Sci. 2 (2000) 405-420.

[36] B. Burczyc, K. A. Wilk, A. Sokolowski, L. Syper, Synthesis and Surface Properties of N-Alkyl-N-methylgluconamides and N-Alkyl-N-methylgluconamides and N-Alkyl-N-methyllactobionamides, J. of Colloid and Interface Science 240 (2001) 552-558.

[37] D.L. Harp, Modifications to the azomethine-H method for determining boron in water, Analytica Chimica Acta 346 (1997) 373-379.

[38] R. N. Sah and P. H. Brown, Boron Determination - A Review of Analytical Methods, Microchemical Journal 56 (1997) 285–304.

[39] L. Huerta, C. Guillem, J. Latorre, A. Beltrán, D. Beltrán, P. Amorós, Large monolithic silica-based macrocellular foams with trimodal pore system, Chem. Commun. (2003) 1448-1449.

[40] J. V. Ros-Lis, R. Casasús, M. Comes, C. Coll, M. D. Marcos, R. Martínez-Máñez, F. Sancenón, J. Soto, P. Amorós, J. El Haskouri, N. Garró, K. Rurack, A mesoporous 3D Hybrid Material with Dual Functionality for Hg^{2+} Detection and Adsorption, Chem. Eur. J. 14 (2008) 8267-8278.

[41] S. Brunauer, P. H. Emmet, E. Teller, Adsorption of Gases in Multimolecular Layers, J. Am. Chem. Soc. 60 (1938) 309 – 319.

[42] E. P. Barret, L. G. Joyner, P. P. Halenda, The Determination of Pore Volume and Area Distributions in Porous Substances. I. Computations from Nitrogen Isotherms, J. Am. Chem. Soc. 73 (1951) 373 – 380.